Numerical Study of a Discontinuous Galerkin Method for Incompressible Two-Phase Flow

Béatrice Rivière [†]

Abstract

This paper presents a high-order numerical method for solving the pressure-saturation formulation of the two-phase flow problem. The saturation and pressure of the wetting phase are approximated by totally discontinuous polynomials of different order. The robustness of the method is shown for homogeneous and heterogeneous porous media.

1 Introduction

The geological structure of the subsurface is highly heterogeneous and for example, contains different rock types, faults, channels and networks of fractures. There is a need for reliable numerical methods that would model the flow and transport of chemical species in heterogeneous porous media. In the oil industry, most reservoir simulators employ finite differences. Though these low order methods are popular and efficient for homogeneous media and regular grids, they lose their stability on highly unstructured meshes and extra care is needed if the properties of the media are highly discontinuous.

This paper presents a high order finite element method that naturally handles unstructured meshes and heterogeneous porous media for solving the two-phase flow problem. The incompressible flow of a wetting phase

[†]301 Thackeray, University of Pittsburgh, Pittsburgh, PA 15260. (riviere@math.pitt.edu).

and a non-wetting phase is mathematically modelled by a system of nonlinear partial differential equations derived from the conservation of mass and momentum equations for each phase. The reader can refer to the book by Helmig [4] for a review of different mathematical models.

In the proposed algorithm, the primary variables are the wetting phase pressure and saturation. They are approximated by discontinuous polynomials of varying degree. The flexibility of discontinuous Galerkin methods has made these methods competitive for modeling flow and transport problems. Some of the advantages include the high order approximation, the easy implementation on unstructured grids, the robustness of the method for equations with discontinuous coefficients and the local mass conservation property. The nonsymmetric formulation was introduced by Oden, Babuška and Baumann [5]; it was analyzed by Rivière, Wheeler and Girault [7] for elliptic problems and by Rivière and Wheeler [9] for transport problems. Applications of nonsymmetric discontinuous Galerkin methods to porous media flow were investigated by Rivière [6], Rivière and Wheeler [8] and Bastian [1].

The outline of the paper is as follows. Section 2 contains the description of the model problem. The numerical scheme is introduced in Section 3. Numerical results are given in Section 4, followed by some concluding remarks.

2 Model Problem

We consider the flow of a wetting phase (such as water) and a non-wetting phase (such as oil) in a porous medium $\Omega \subset \mathbb{R}^2$ over a time period $(0, T)$. For a given integer $N > 0$, let $\Delta t = T/N$, let $t^0 = 0$ and $t^n = t^0 + n\Delta t$. Denote s_w^n (resp. p_w^n) the water saturation (resp. pressure) at time t^n. Similarly, s_o^n and p_o^n denote the oil saturation and pressure at t^n. The model problem is: given (p_w^n, s_w^n), find (p_w^{n+1}, s_w^{n+1}) such that

$$-\nabla \cdot (\boldsymbol{K}(\lambda_o^n + \lambda_w^n)\nabla p_w^{n+1}) = -\nabla \cdot (\boldsymbol{K}\lambda_o^n |p_c'(s_w^n)|\nabla s_w^n), \tag{1}$$

$$\frac{\phi}{\Delta t}s_w^{n+1} - \nabla \cdot (\boldsymbol{K}\frac{\lambda_o^n \lambda_w^n}{\lambda_o^n + \lambda_w^n}|p_c'(s_w^n)|\nabla s_w^{n+1}) = \frac{\phi}{\Delta t}s_w^n - \nabla \cdot (\frac{\lambda_w^n}{\lambda_o^n + \lambda_w^n}\boldsymbol{u}^n). \tag{2}$$

The coefficients in (1) and (2) are defined below:

- The permeability $\mathbf{K}$ is a symmetric positive definite tensor, obtained from a macroscopic averaging of the microscopic features of the medium.

Therefore, it is discontinuous in the space variable and can vary over several orders of magnitude.

- λ_o^n and λ_w^n are the mobilities of oil and water respectively at time t^n. Mobilities are the ratios of relative permeabilities by the viscosities $\lambda_\alpha = k_{r_\alpha}/\mu_\alpha$. The viscosities are assumed constant throughout the domain, and the relative permeabilities are functions that depend on the wetting phase saturation s_w in a non-linear fashion. In this work, the commonly used Brooks-Corey model [2] is considered.

  $$k_{rw}(s) = s^{\frac{2+3\theta}{\theta}}, \quad k_{ro}(s) = (1-s)^2(1-s^{\frac{2+\theta}{\theta}}).$$

  This model introduces an additional parameter $\theta \in [0.2, 3.0]$, characterizing the inhomogeneity of the medium.

- $p_c = p_o - p_w$ is the capillary pressure, that is the difference of the pressures in the two phases. For the Brooks-Corey model, we have

  $$p_c(s) = p_d s^{-\frac{1}{\theta}},$$

  where p_d is the capillary pressure needed to displace the fluid from the largest pore.

- ρ_o, ρ_w, ϕ are the phase densities and the porosity respectively. They are chosen constant in the numerical examples.

- $\boldsymbol{u}^n$ is the total velocity at t^n defined by $\boldsymbol{u}^n = -\boldsymbol{K}\lambda_o^n p_c'(s_w^n)\nabla s_w^n - \boldsymbol{K}(\lambda_o^n + \lambda_w^n)\nabla p_w^n$.

The approximation of the oil saturation and pressure are derived from the constitutive equations.

$$s_o^{n+1} = 1 - s_w^{n+1}, \quad p_o^{n+1} = p_c(s_w^{n+1}) + p_w^{n+1}.$$

Let $\boldsymbol{\nu}$ denotes the outward normal to $\partial\Omega$. Assume the boundary of the domain is divided into three disjoint open sets $\partial\Omega = \Gamma_N \cup \Gamma_+ \cup \Gamma_-$ on which the following boundary conditions apply:

$$p_w^{n+1} = p_{\text{dir}}^-, \qquad (s_w^{n+1}\boldsymbol{u}^n - \boldsymbol{K}\frac{\lambda_o^n\lambda_w^n}{\lambda_o^n+\lambda_w^n}|p_c'(s_w^n)|\nabla s_w^{n+1})\cdot\boldsymbol{\nu} = s_{\text{in}}\boldsymbol{u}^n\cdot\boldsymbol{\nu}, \quad \text{on} \quad \Gamma_-,$$

$$p_w^{n+1} = p_{\text{dir}}^+, \quad \boldsymbol{K}\frac{\lambda_o^n\lambda_w^n}{\lambda_o^n+\lambda_w^n}|p_c'(s_w^n)|\nabla s_w^{n+1}\cdot\boldsymbol{\nu} = 0, \quad \text{on} \quad \Gamma_+,$$

$$\boldsymbol{K}(\lambda_o^n+\lambda_w^n)\nabla p_w^{n+1}\cdot\boldsymbol{\nu} = 0, \quad \boldsymbol{K}\frac{\lambda_o^n\lambda_w^n}{\lambda_o^n+\lambda_w^n}|p_c'(s_w^n)|\nabla s_w^{n+1}\cdot\boldsymbol{\nu} = 0, \quad \text{on} \quad \Gamma_N.$$

In the model (1)-(2), the nonlinearity has been removed by time-lagging the coefficients. In the next section, a fully discrete system is obtained by discretizing in space.

3 Numerical Method

Let $\mathcal{E}_h = \{E\}_E$ be a non degenerate triangular subdivision of Ω, with maximum diameter h. Let Γ_h be the union of the open sets that coincide with interior edges of elements of $\mathcal{E}_h$. Let e denote a segment of Γ_h shared by two elements E^k and E^l of $\mathcal{E}_h$; we associate with e, once and for all, a unit normal vector $\boldsymbol{\nu}_e$ directed from E^k to E^l $(k > l)$ and we define formally the jump and average of a function ψ on e by:

$$[\psi] = (\psi|_{E^k})|_e - (\psi|_{E^l})|_e, \quad \{\psi\} = \frac{1}{2}(\psi|_{E^k})|_e + \frac{1}{2}(\psi|_{E^l})|_e.$$

If e is adjacent to $\partial\Omega$, then the jump and the average of ψ on e coincide with the trace of ψ on e and the normal vector $\boldsymbol{\nu}_e$ coincides with the outward normal $\boldsymbol{\nu}$. For a given integer $r \geq 0$, the discontinuous finite element space is

$$\mathcal{D}_r(\mathcal{E}_h) = \{v \in L^2(\Omega) : v|_E \in I\!P_r(E) \quad \forall E \in \mathcal{E}_h\}.$$

We approximate the water pressure and saturation by discontinuous polynomials of total degrees r_p and r_s respectively. Let P_w^n and S_w^n be the numerical solutions at time t^n. Assuming that (P_w^n, S_w^n) is known, the approximations at the next time step (P_w^{n+1}, S_w^{n+1}) are obtained in three stages.
Stage 1: Computation of water pressure.

$$\sum_{E\in\mathcal{E}_h}\int_E \boldsymbol{K}(\lambda_o^n+\lambda_w^n)\nabla P_w^{n+1}\cdot\nabla v - \sum_{e\in\Gamma_h\cup\Gamma_+\cup\Gamma_-}\int_e\{\boldsymbol{K}(\lambda_o^n+\lambda_w^n)\nabla P_w^{n+1}\cdot\boldsymbol{\nu}_e\}[v]$$
$$+\sum_{e\in\Gamma_h\cup\Gamma_+\cup\Gamma_-}\int_e\{\boldsymbol{K}(\lambda_o^n+\lambda_w^n)\nabla v\cdot\boldsymbol{\nu}_e\}[P_w^{n+1}] = \sum_{E\in\mathcal{E}_h}\int_E \boldsymbol{K}\lambda_o(S_w^n)|p_c'(S_w^n)|\nabla S_w^n\cdot\nabla v$$
$$-\sum_{e\in\Gamma_h\cup\Gamma_+\cup\Gamma_-}\int_e \boldsymbol{K}\lambda_o(\tilde{S}_w^n)|p_c'(\tilde{S}_w^n)|\nabla\tilde{S}_w^n\cdot\boldsymbol{\nu}_e[v] + \int_{\Gamma_+\cup\Gamma_-}(\boldsymbol{K}(\lambda_o^n+\lambda_w^n)\nabla v\cdot\boldsymbol{\nu})p_{\rm dir}, \quad \forall v\in\mathcal{D}_{r_p}(\mathcal{E}_h).$$

Stage 2: Computation of water saturation.

$$\int_\Omega \frac{\phi}{\Delta t} S_w^{n+1} z + \sum_{E\in\mathcal{E}_h} \int_E \boldsymbol{K} \frac{\lambda_o^n \lambda_w^n}{\lambda_o^n + \lambda_w^n} |p_c'(S_w^n)| \nabla S_w^{n+1} \cdot \nabla z - \int_{\Gamma_-} S_w^{n+1} \boldsymbol{U}^n \cdot \boldsymbol{\nu} z$$

$$- \sum_{e\in\Gamma_h\cup\Gamma_+} \int_e \{\boldsymbol{K} \frac{\lambda_o^n \lambda_w^n}{\lambda_o^n + \lambda_w^n} |p_c'(S_w^n)| \nabla S_w^{n+1} \cdot \boldsymbol{\nu}_e\}[z] + \sum_{e\in\Gamma_h\cup\Gamma_+} \int_e \{\boldsymbol{K} \frac{\lambda_o^n \lambda_w^n}{\lambda_o^n + \lambda_w^n} |p_c'(S_w^n)| \nabla z \cdot \boldsymbol{\nu}_e\}[S_w^{n+1}]$$

$$= \int_\Omega \frac{\phi}{\Delta t} S_w^n z + \sum_{E\in\mathcal{E}_h} \int_E \frac{\lambda_w(S_w^n)}{\lambda_o(S_w^n) + \lambda_w(S_w^n)} \boldsymbol{U}^n \cdot \nabla z - \sum_{e\in\Gamma_h\cup\Gamma_+\cup\Gamma_-} \int_e \frac{\lambda_w(\tilde{S}_w^n)}{\lambda_o(\tilde{S}_w^n) + \lambda_w(\tilde{S}_w^n)} \{\boldsymbol{U}^n \cdot \boldsymbol{\nu}_e\}[z]$$

$$- \sum_{e\in\Gamma_h\cup\Gamma_+\cup\Gamma-} \int_e \{\boldsymbol{K} \lambda_w^n \nabla z \cdot \boldsymbol{\nu}_e\}[P_w^n] - \int_{\Gamma_-} s_{\text{in}} \boldsymbol{U}^n \cdot \boldsymbol{\nu} z, \quad \forall z \in \mathcal{D}_{r_s}(\mathcal{E}_h).$$

where the approximation of the total velocity is

$$\boldsymbol{U}^n = -\boldsymbol{K} p_c'(S_w^n) \nabla S_w^n - \boldsymbol{K}(\lambda_w(S_w^n) + \lambda_o(S_w^n)) \nabla P_w^n.$$

Stage 3: Application of slope limiters if necessary. For triangular elements, the slope limiter developped by Durlofsky, Engquist and Osher [3] is used.

The quantity $\tilde{S}_w^n$ is the upwind value of the water saturation with respect to the normal component of the velocity $\boldsymbol{U}^n$.

$$\forall e = \partial E^k \cap \partial E^l, \quad k > l, \quad \tilde{S}_w^n = \begin{cases} S_w^n|_{E^k} & \text{if } \{\boldsymbol{U}^n\} \cdot \boldsymbol{\nu}_e \geq 0, \\ S_w^n|_{E^l} & \text{if } \{\boldsymbol{U}^n\} \cdot \boldsymbol{\nu}_e < 0. \end{cases}$$

It is easy to show that the numerical scheme is consistent with the mathematical model problem. An important property of our scheme is that it is locally mass conservative. This is easily seen by fixing an element E and a test function v equal to 1 on E and zero elsewhere. For simplicity, let us assume that E is an interior element in Ω. The pressure equation solved at stage 1 becomes:

$$- \int_{\partial E} \{\boldsymbol{K}(\lambda_o(S_w^n) + \lambda_w(S_w^n)) \nabla P_w^{n+1} \cdot \boldsymbol{\nu}_E\} + \int_{\partial E} \boldsymbol{K} \lambda_o(\tilde{S}_w^n) |p_c'(\tilde{S}_w^n)| \nabla \tilde{S}_w^n \cdot \boldsymbol{\nu}_E = 0,$$

which is an approximation of the local mass conservation of the total velocity. The scheme naturally handles discontinuous permeability tensors, by averaging the fluxes at the discontinuity points.

4 Simulations

The numerical scheme is applied to the quarter-five spot waterflooding problem, which is a widely used benchmark problems for reservoir simulations. The domain Ω is embedded in the square $(0, 300m)^2$. Water is injected through injection wells and NAPL is produced at the production wells. The wells are modeled with boundary conditions on the saturation and pressure, prescribed at the well bore:

$$p_w = 3.45e^6 Pa, \quad s_{\text{in}} = 0.4, \quad \text{on} \quad \Gamma_-$$
$$p_w = 2.41e^6 Pa, \quad \text{on} \quad \Gamma_+$$

The entry pressure is $p_d = 5000Pa$. The fluid properties are

$$\rho_w = \rho_o = 1000kg/m^3, \quad \mu_o = 0.002kg/(ms), \quad \mu_w = 0.0005kg/(ms), \quad \phi = 0.2.$$

We first consider the case where the injection well is located at the bottom left corner, and the production well located at the top right corner. On the rest of the boundary Γ_N, zero Neumann boundary conditions are imposed. The domain is subdivided into triangular elements and a description of the problem and the coarse mesh are given in Fig. 1. There are 66 triangles in the coarse mesh.

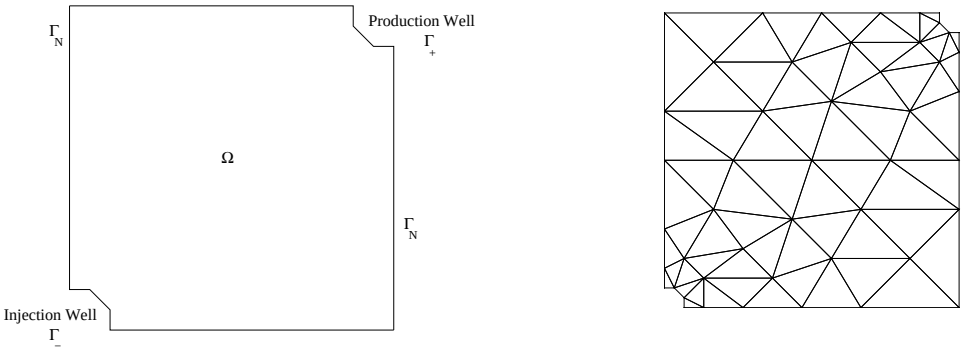

Figure 1: Configuration 1: Domain and boundary conditions (left) and coarse mesh (right).

Second, we assume that there are two injection wells located at the bottom left and top right corners, and two production wells located at the bottom right and top left corners. The domain and coarse mesh for this second case are given in Fig. 2. There are 92 triangles in the coarse mesh.

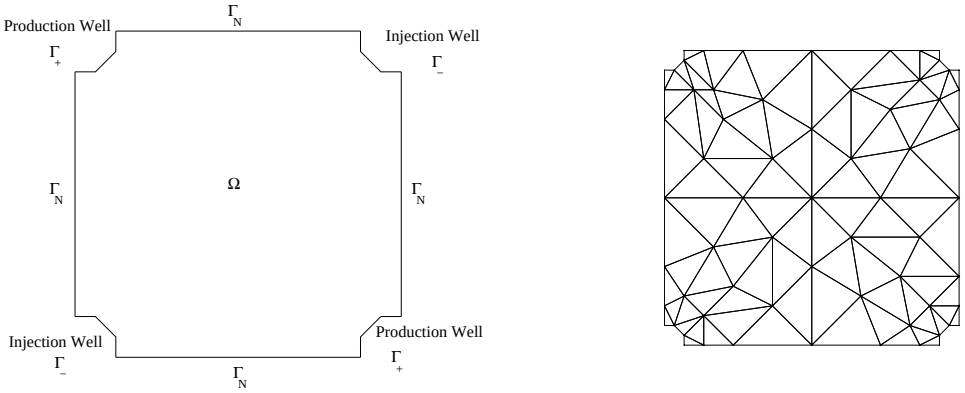

Figure 2: Configuration 2: Domain and boundary conditions (left) and coarse mesh (right).

As further notation, we refer to the coarse mesh as mesh h_0 and to the successively refined meshes as mesh h_j for $j > 0$.

4.1 The homogeneous porous medium

The permeability field is simply $\boldsymbol{K} = k\boldsymbol{I}$ with $k = 1.e^{-11}m^2$. We first consider the case where there is no capillary pressure for the configuration 1. The Brooks-Corey parameter θ is taken to be 2.0 for the phase mobilities. The water saturation and pressure on the coarse mesh h_0 are given on Fig. 3 at 100 and 200 days. The saturation is approximated by piecewise constants and the pressure by piecewise quadratics. In this case, no slope limiter is used. Convergence of the numerical solution is shown on Fig. 4 where we refined the mesh successively. Note that the saturation fronts are quite sharp, and only extends over a layer of one to two elements wide. Fig. 5 shows the pressure contours in a three-dimensional perspective. The gradient of pressure drives the flow from the injection well to the production well.

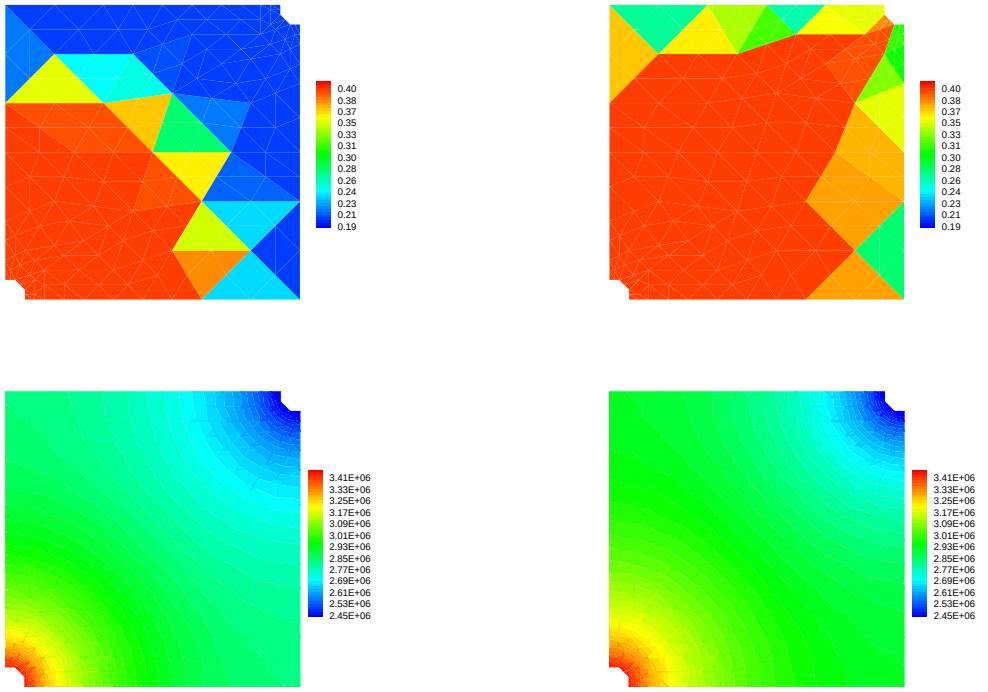

Figure 3: Saturation and pressure contours at 100 days (left column) and 200 days (right column), on coarse mesh h_0.

Second, we add the capillary pressure terms. The Brooks-Corey parameter θ is taken to be 3.0. The water saturation and pressure on meshes h_0 are given on Fig. 6 at different times. They are approximated by piecewise linears and piecewise quadratics respectively. The contours on the refined mesh h_1 are shown in Fig. 7

We next compare the simulations obtained by changing the Brooks-Corey parameter to $\theta = 0.5$. The wetting phase is displaced more slowly than for large θ (see Fig. 8).

We then consider the configuration 2, and repeat the numerical experiments for $\theta = 3.0$. The saturation and pressure on the coarse mesh are shown in Fig. 9. The saturation is shown at 25 and 50 days on the mesh h_2. The saturation fronts are sharp. The contours are symmetric because of the homogeneity of the medium and the symmetry of the boundary conditions.

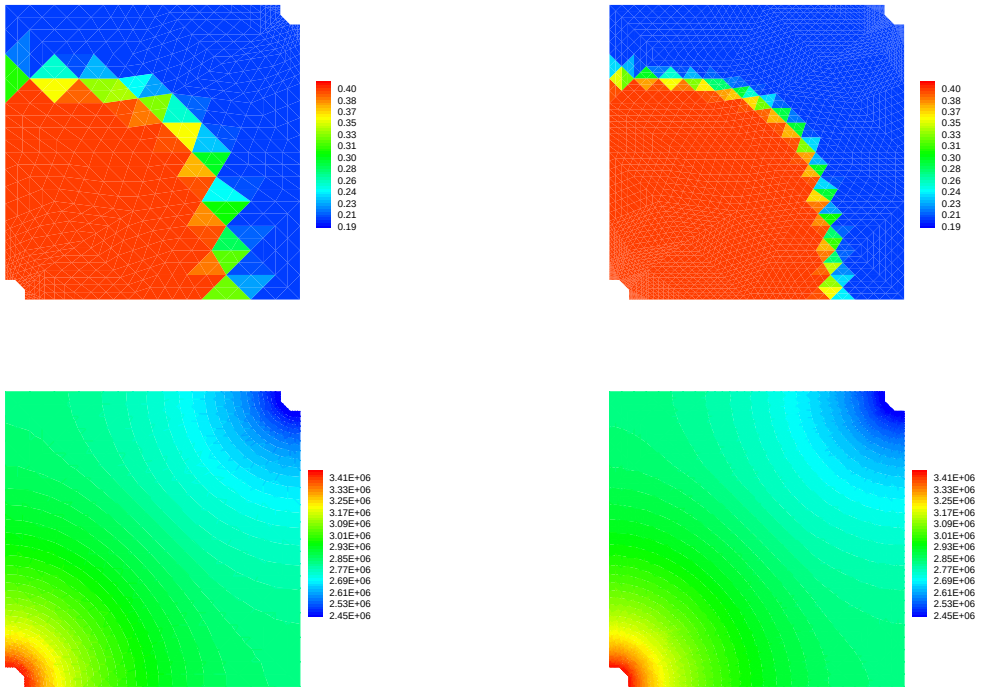

Figure 4: Saturation and pressure contours at 100 days on mesh h_1 (left column) and mesh h_2 (right column).

After 100 days, the wetting phase has flooded the entire domain.

4.2 The heterogeneous porous medium

In this example, the underlying rock has inclusions of permeability that is 100 times lower than the rock matrix (see Fig. 11). The inclusions are in blue, the rock matrix in red. Here, the capillary pressure is included, and the Brooks-Corey parameter is $\theta = 3.0$. Piecewise linears are used for the saturation, and piecewise quadratics are used for the pressure. For the first configuration, the saturation and pressure contours are obtained on the meshes h_0 and h_1 at 100 days (see Fig. 12). The saturation fronts are sharp and the wetting phase avoids the regions of low permeability, as expected, even on the coarse mesh. There is very little numerical diffusion.

Next, for the second configuration, Fig. 13 shows the saturation contours obtained on meshes h_0, h_1 and h_2 at 50 and 100 days. As before, one concludes that the saturation fronts are quite sharp. The regions of low permeability play the role of barriers for the flooding of the wetting phase. In all these examples, the water saturation decreases from its injected value to its initial value over a layer of one to two elements. For completeness, the pressure contours are shown on meshes h_0 and h_2 at 100 days (see Fig. 14).

5 Conclusions

We presented a numerical method that employed discontinuous polynomial approximations, for solving the wetting phase pressure-saturation formulation of the two-phase flow. We applied the method to the quarter-five spot flooding, where the method numerically converged. We showed the robustness of the method on coarse unstructured meshes and for heterogeneous media.

References

[1] P. Bastian. High order discontinuous Galerkin methods for flow and transport in porous media. *Challenges in Scientific Computing CISC 2002*, ed. E. Bansch, **35**, LNCSE 2003.

[2] R.H. Brooks and A.T. Corey. Hydraulic properties of porous media. *Hydrol. Pap.*, **3**, Fort Collins, 1964.

[3] L.J. Durlofsky, B. Engquist and S. Osher. Triangle based adaptive stencils for the solution of hyperbolic conservation laws. *Journal of Computational Physics*, **98**, 64–73, 1992.

[4] R. Helmig. *Multiphase flow and transport processes in the subsurface.* Springer. 1997.

[5] J.T. Oden, I. Babuška and C. Baumann. A discontinuous hp finite element method for diffusion problems. *Journal of Computational Physics*, **146**, 491–519, 1998.

[6] B. Rivière. *Discontinuous Galerkin methods for solving the miscible displacement problem in porous media.* Ph.D. Thesis, The University of Texas at Austin, May 2000.

[7] B. Rivière, M. Wheeler and V. Girault. Improved energy estimates for interior penalty, constrained and discontinuous Galerkin methods for elliptic problems I. *Computational Geosciences*, **3**, 337–360, 1999.

[8] B. Rivière and M.F. Wheeler. Discontinuous Galerkin methods for flow and transport problems in porous media. *Communications in Numerical Methods in Engineering*, **18**, 63–68, 2002.

[9] B. Rivière and M.F. Wheeler. Non conforming methods for transport with nonlinear reaction. *Proceedings of an AMS-IMS-SIAM Joint Summer Research Conference on Fluid Flow and Transport in Porous Media: Mathematical and Numerical Treatment*, ed. Zhangxin Chen and Richard E. Ewing, 421–432, 2002.

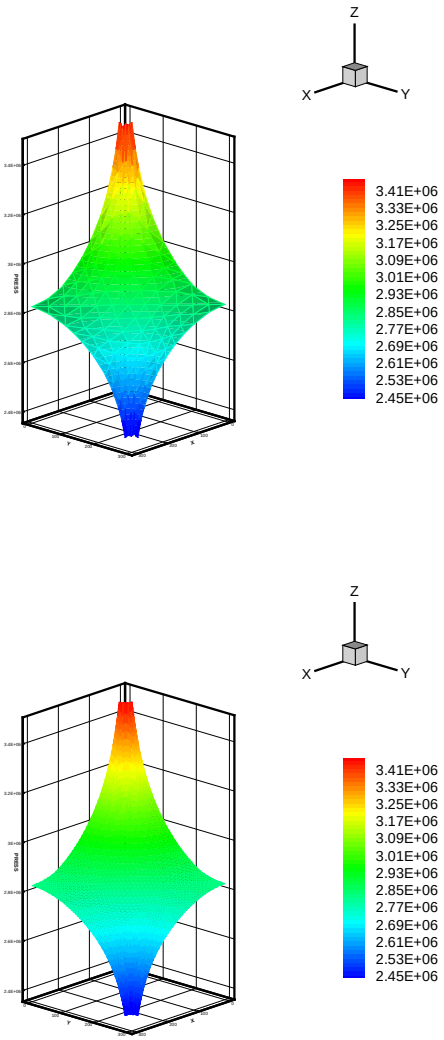

Figure 5: Three-dimensional view of pressure contours at 100 days on meshes h_0 (left) and h_2 (right).

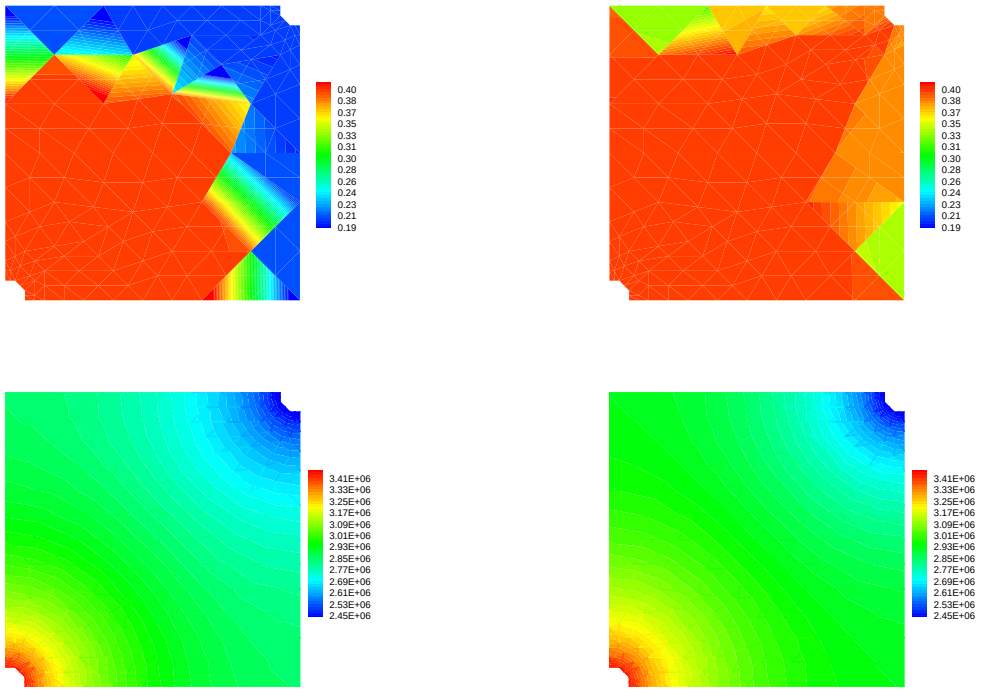

Figure 6: Configuration 1. Saturation and pressure contours at 100 days (left column) and 200 days (right column), on mesh h_0.

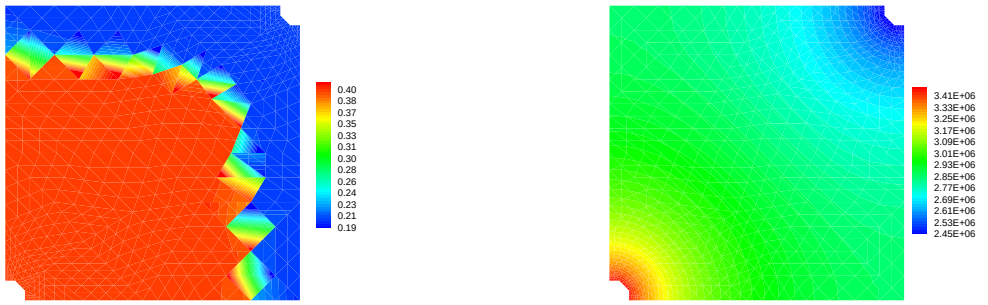

Figure 7: Configuration 1. Saturation (left) and pressure (right) contours at 100 days on mesh h_1.

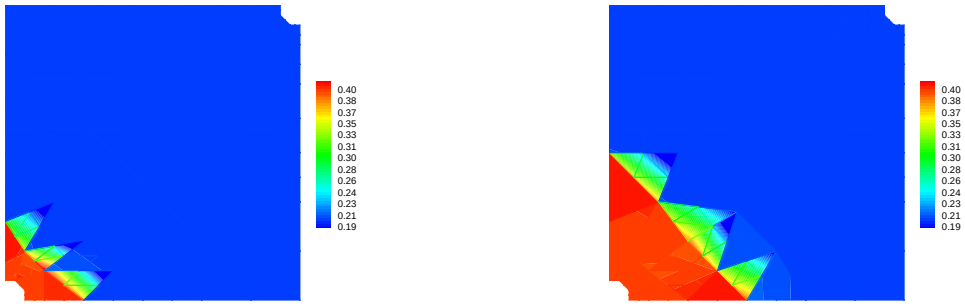

Figure 8: Configuration 1. Saturation contours at 100 days (left) and 400 days (right) on mesh h_0.

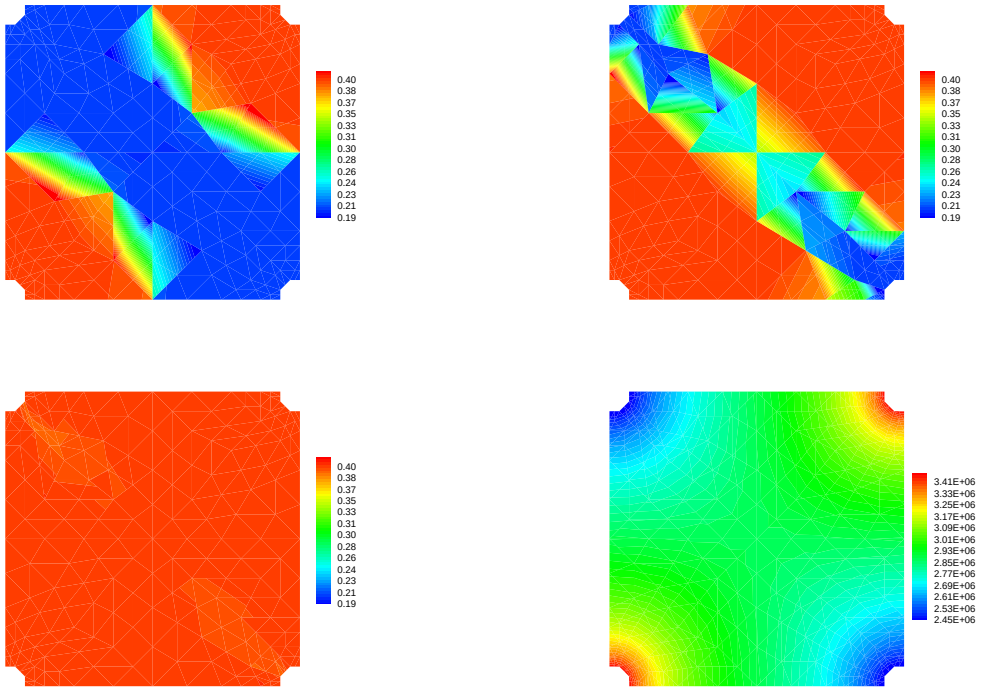

Figure 9: Configuration 2. Saturation contours at 25 (top left), 50 (top right) and 100 (bottom left) days on mesh h_0. Pressure contour at 50 days (bottom right).

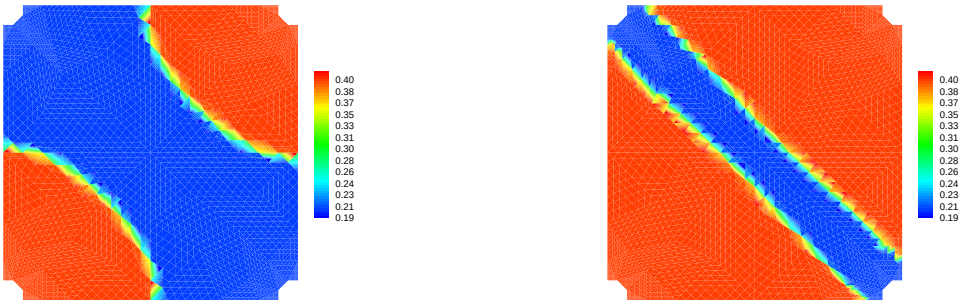

Figure 10: Configuration 2. Saturation contours at 25 (left) and 50 (right) days on mesh h_2.

Figure 11: Discontinuous permeability field: configuration 1 (left) and configuration 2 (right).

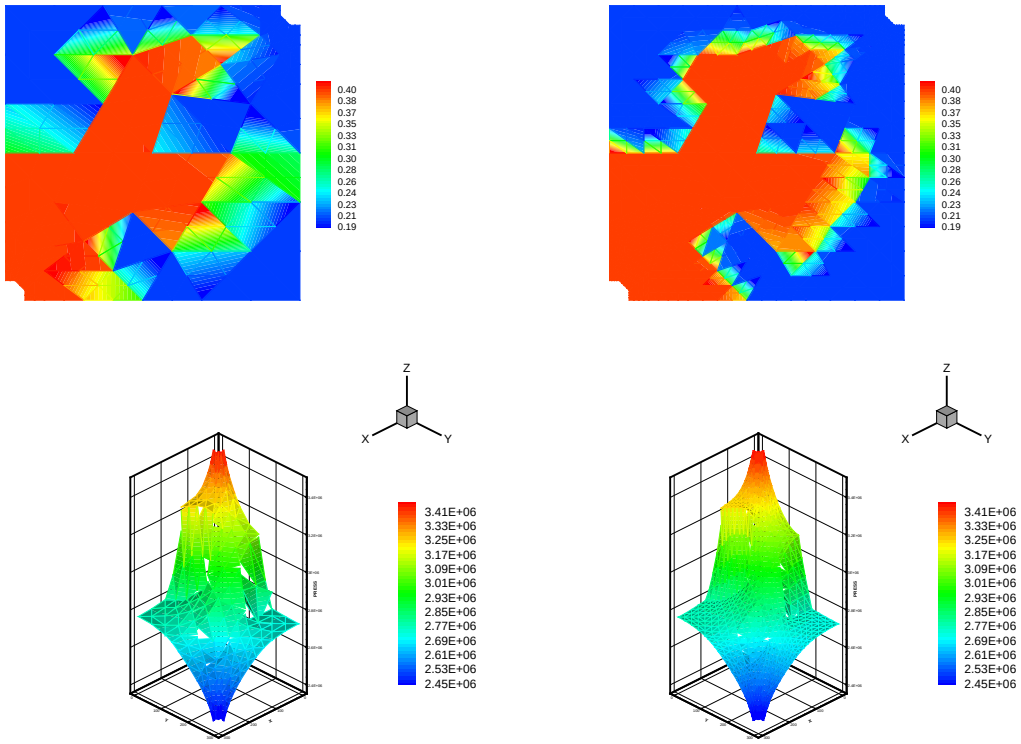

Figure 12: Configuration 1. Heterogeneous medium. Saturation and pressure contours at 100 days on meshes h_0 (left column) and h_1 (right column).

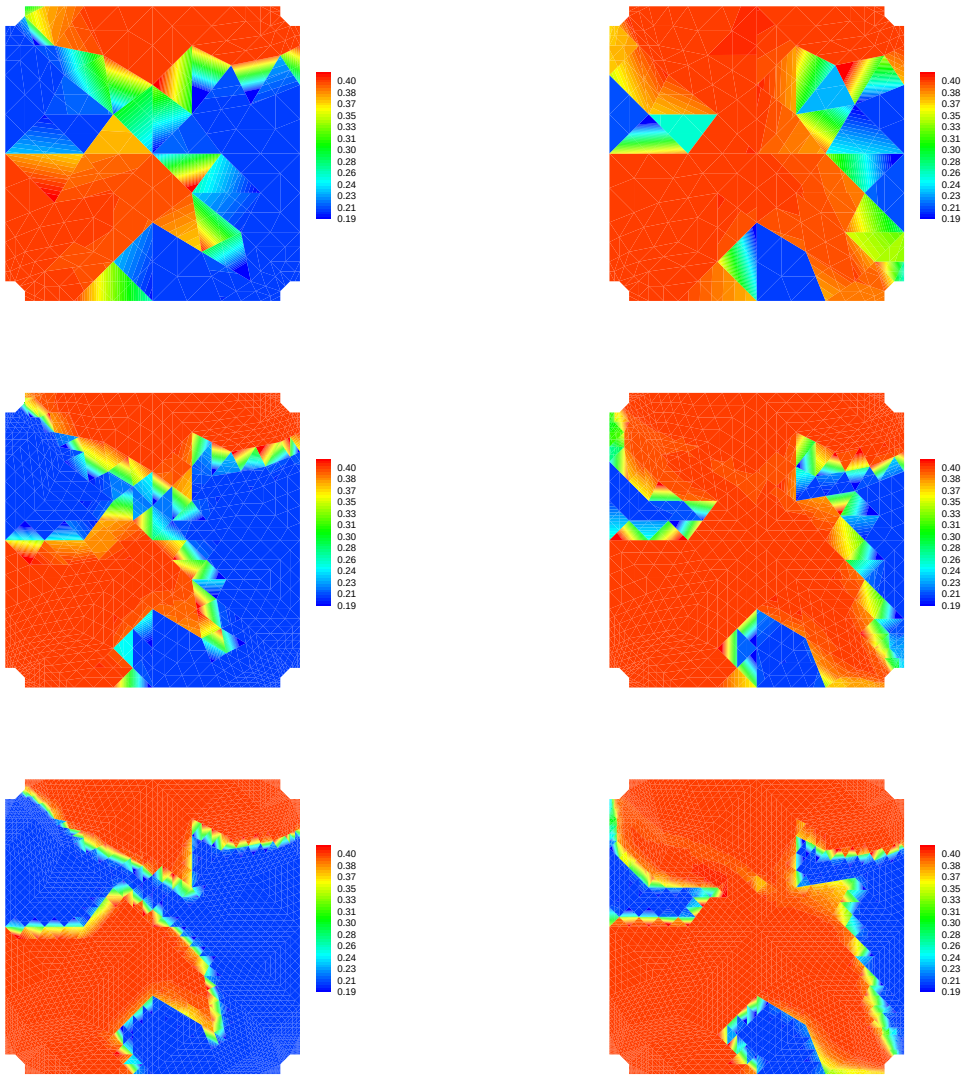

Figure 13: Configuration 2. Heterogeneous medium. Saturation contours at 50 (left column) and 100 (right column) days on mesh h_0 and mesh h_1, h_2

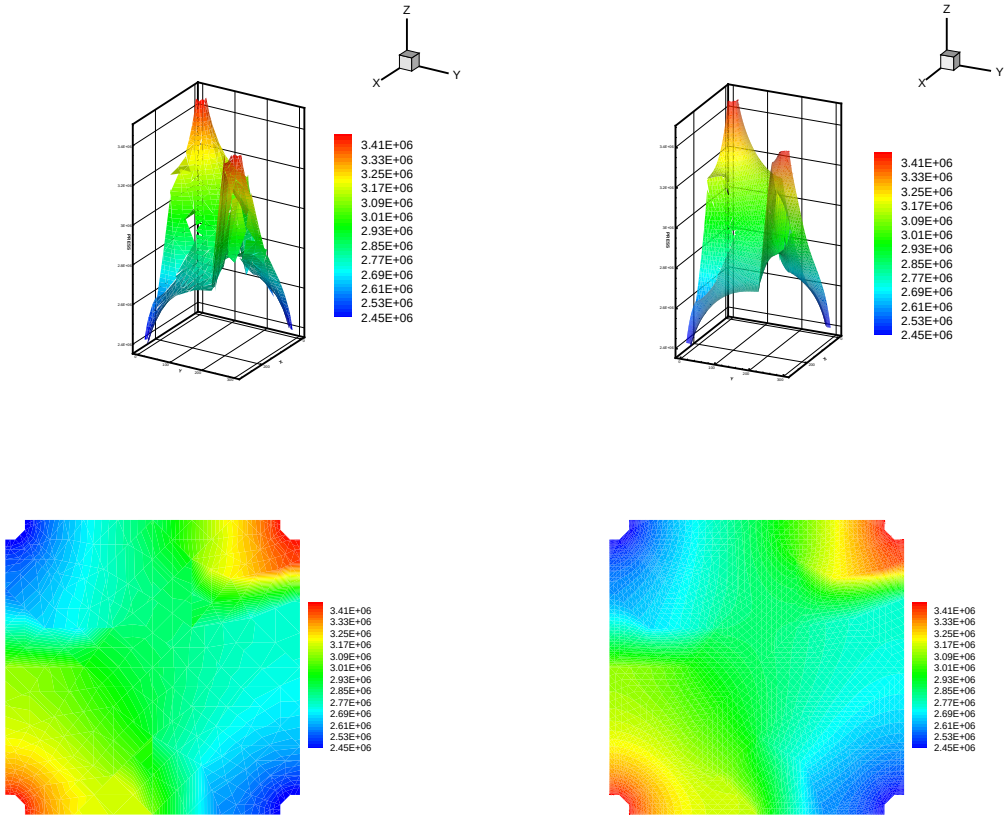

Figure 14: Configuration 2. Heterogeneous medium. Three-dimensional and two-dimensional views of pressure contours at 100 days on mesh h_0 (left column) and mesh h_2 (right column).